Model-Based Analysis of a Diesel Generator Operating in islanded Mode under Dynamic Load Conditions

Daniel Jörss[1], Maximilian Ringel[1], Bert Buchholz[2], Christian Fink[1*]

[1]Department of Mechanical / Process and Environmental Engineering, Wismar University of Applied Sciences, Philipp-Müller-Str. 14, 23966 Wismar, Germany; [*]*Christian.Fink@hs wismar.de*

[2]Chair of Piston Machines and Internal Combustion Engines, Rostock University, Albert-Einstein-Straße 2, 18059 Rostock, Germany

SNE 36(1), 2026, 37-44, DOI: 10.11128/sne.36.tn.10766
Selected ASIM GMMS/STS 2025 Postconf. Publ.: 2025-10-22
Rec. Revised English: 26-02-11; Accepted: 2026-02-20
SNE - Simulation Notes Europe, ARGESIM Publisher Vienna
ISSN Print 2305-9974, Online 2306-0271, www.sne-journal.org

Abstract. This paper presents a simulation model of a power generation unit consisting of an internal combustion engine, a synchronous generator and electrical loads. The internal combustion engine model is primarily based on thermodynamic and mechanical submodels that describe the processes occurring inside the engine. For the combustion model, a phenomenological modeling approach is applied, in which the injection profile obtained from a coupled hydraulic simulation serves as an input to the combustion model. The synchronous generator is described using a per-unit (PU) based Simscape™ model. By coupling the two models, the interaction between the internal combustion engine and the synchronous generator is simulated in order to analyze the overall behavior of the power generation unit under various operating conditions. The overall model enables a very accurate prediction of the generator behavior and serves as a basis for the optimization of operating strategies and system configuration. For validation of the simulation model, measurements were carried out on a power generator under varying load conditions. The simulation results show a high level of agreement with the measurement data under dynamic operating conditions.

Introduction

In the course of the energy transition, decentralized power generation is gaining increasing importance.

This also applies to combined heat and power (CHP) units, which simultaneously generate heat and electricity and therefore exhibit high overall efficiency. The core of such systems typically consists of internal combustion engines, which can be operated in a CO_2-neutral manner in the future due to the increasing availability of hydrogen. The operation of power generators in isolated grids under dynamic load conditions imposes high requirements on the operating behavior of the driving internal combustion engine.

In conventional configurations, where the engine is directly coupled to a synchronous generator, load fluctuations can lead to speed variations of the unit and, consequently, to fluctuations in grid frequency. Since many electrical consumers are highly sensitive to frequency deviations, it is essential to keep these within narrow limits.

Therefore, especially manufacturers of larger generator sets are required to quantify the effects of possible load scenarios on the grid frequency provided by the generator already at an early design stage.

Against this background, a simulation model was developed that enables the calculation of the operational behavior of an internal combustion engine in combination with a generator and a variable electrical load scenario based on physical principles.

The model is based on a crank-angle-resolved process calculation in order to obtain a more precise description of the system behavior and to enable optimization of the system configuration with respect to a wide range of parameters.

In this paper, the model of a power generation unit is presented and the obtained simulation results are compared with experimental data from a test bench.

1 Internal Combustion Engine Model

For the simulation environment of the internal combustion engine, a modeling approach based on established submodels was selected.

In this zero-dimensional (0D) model, the combustion chamber is considered as an ideally mixed system at any point in time, and the state variables pressure and temperature are represented as functions of time or crank angle.

Using the energy balance according to the first law of thermodynamics, the change in internal energy dU within the combustion chamber can be described as follows [1]:

$$\frac{dU}{dt} = -p\frac{dV}{dt} + \frac{dQ_B}{dt} - \frac{dQ_W}{dt} + h_I\frac{dm_I}{dt} - h_E\frac{dm_E}{dt} \quad (1)$$

The first term represents the work performed on the piston in the form of volume change work $-p\frac{dV}{dt}$. Furthermore, $\frac{dQ_B}{dt}$ denotes the heat release due to combustion, $\frac{dQ_W}{dt}$ the wall heat transfer, $h_I\frac{dm_I}{dt}$ the enthalpy flux through the intake valve, and $h_E\frac{dm_E}{dt}$ the enthalpy flux through the exhaust valve [2].

To solve the mass and energy balances, models were implemented for the heat release due to combustion (burn rate), heat transfer between the in-cylinder gas and the combustion chamber walls, the gas exchange process, and the change in internal energy within the cylinder.

The calculation of the internal energy is based on the caloric equation of state for ideal gases:

$$du = c_v \cdot dT \quad (2)$$

The specific heat capacity c_v is determined using a component-based model according to Grill [3]. In this approach, the in-cylinder gas is assumed to be a mixture of ideal gas species. A prerequisite is the prior calculation of the equilibrium composition of the in-cylinder gas as a function of temperature, air–fuel ratio, and pressure.

Based on this approach, the specific internal energy is used to determine the specific heat capacity c_v according to Equation (3) [3]:

$$c_v = \left(\frac{\partial u}{\partial T}\right)_p + \left(\frac{\partial u}{\partial p}\right)_T \cdot \frac{p}{T} \quad (3)$$

1.1 Combustion model

A key component in modeling the in-cylinder process is the combustion model. This model describes the temporal evolution of heat release from the chemical energy stored in the fuel (reaction enthalpy released during combustion).

Various modeling approaches can be used to represent the burn rate, including phenomenological or empirical burn rate models.

In the present simulation model, a combined phenomenological combustion model based on the approaches of Barba [4] and Chmela [5] is employed. The input variable for this model is the injection rate, which is calculated using an implemented injector model [6].

The calculation of the combustion process is based on two submodels: one for the pilot combustion and one for the main combustion. For the combustion of the pilot injection, a spherical propagation of the flame front originating from a single ignition point is assumed.

The flame radius is determined by the turbulent flame speed s_{turb}. The flame surface area can be expressed as follows [7]:

$$A_{Flame} = 4 \cdot \pi \cdot r_{Flame}^2 \quad (4)$$

Assuming a homogeneous air–fuel mixture, the mass burning rate for turbulent combustion originating from a single ignition point can be described by:

$$\dot{m}_{FuelBurn\ I} = k_1 \cdot \rho_{ub} \cdot s_{turb} \cdot A_{Flame} \quad (5)$$

However, it can be assumed that ignition does not occur at only one localized point in the combustion chamber, especially once the pilot combustion has progressed. Therefore, following [4,7,8], a second approach for modeling the combustion process is implemented:

$$\dot{m}_{FuelBurn\ II} = k_2 \cdot \frac{1}{\Lambda_{mc}^2} \cdot \frac{s_{turb}}{r_{mc}} \cdot m_{FuelVap} \quad (6)$$

The total burned fuel mass is obtained from the superposition of Equations (5) and (6) [8]:

$$\dot{m}_{FuelBurn} = \frac{\dot{m}_{FuelBurn\ I} \cdot \dot{m}_{FuelBurn\ II}}{\dot{m}_{FuelBurn\ I} + \dot{m}_{FuelBurn\ II}} \quad (7)$$

The combustion model for the main injection is also described using two submodels: one for premixed combustion and one for diffusion-controlled combustion.

First, the spray penetration depth S is calculated using an approach proposed by Najar [9]:

$$S_{\rho_g} = 265,7 \cdot \left(\frac{m_f}{\sqrt{Q_{hyd}}} \right)^{0,445} \cdot \rho_g^{-0,387} \tag{8}$$

Figure 1 illustrates the schematic representation of the spray for different air–fuel ratio regions in the combustion model. The region close to the nozzle represents a fuel-rich zone with limited air availability. As the spray penetrates further into the combustion chamber, the local air–fuel ratio increases accordingly.

Based on the lambda-dependent regions, a mixture volume V_{mix} can be determined in which the evaporated fuel and the amount of air defined by the local air–fuel ratio are present [5]:

$$V_{mix} = m_F \left(\frac{1}{\rho_{F,vap}} + \frac{\lambda \cdot L_{min}}{\rho_{Air}} \right) \tag{9}$$

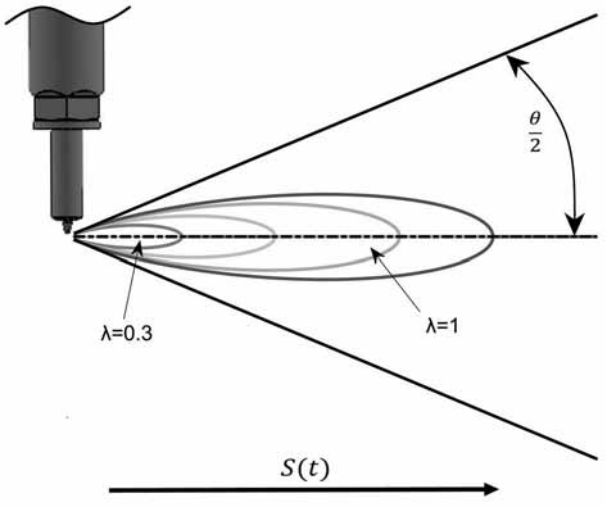

Figure 1: Schematic representation of the air–fuel ratio regions within the injection spray.

Within the model, two fuel pools are distinguished. The amount of fuel injected during the ignition delay period is assigned to the premixed combustion, whereas the fuel injected after the start of combustion is attributed to diffusion-controlled combustion.

The ignition delay is divided into a physical and a chemical part [4]:

$$\tau_{ID} = \tau_{ID,phy} + \tau_{ID,chem} \tag{10}$$

The individual components are calculated using Equations (11) and (12):

$$\tau_{ID,phy} = c_0 \cdot {u_{Drop0}}^{-1.68} \cdot {d_{D.eff}}^{0.88} \tag{11}$$

$$\tau_{ID,chem} = c_1 \cdot \left(\frac{p_{cyl}}{p_0} \right)^{c_2} \cdot {\lambda_{Zn}}^{c_3} \cdot e^{\frac{T_{Act}}{T_G}} \tag{12}$$

To account for the temporal variation of pressure and temperature during the ignition delay, the following integral formulation is applied:

$$1 = \int_{t_{SOI}}^{t_{SOC}} \frac{1}{\tau_{ID}} dt \tag{13}$$

The ignition event occurs when the integral reaches unity. After the start of combustion, the heat release rate of the premixed combustion phase is calculated according to [5]:

$$\frac{dQ_{B.Pre}}{dt} = c_{pre,1} \cdot \lambda_{pre} \cdot L_{min} \cdot e^{-\frac{c_{pre,2} \cdot T_{Act}}{T_G}} \cdot \frac{{m_{f,Pre}}^2}{V_{mix}} \cdot H_U \cdot (t - t_{SOC})^2 \tag{14}$$

The diffusion-controlled combustion is modeled using a frequency-based approach according to Barba [4] and is described by:

$$\frac{dQ_{B.Diff}}{dt} = \frac{u'}{l_{Diff}} \cdot m_{FuelVap} \cdot H_U \tag{15}$$

By introducing a characteristic mixing length l_{Diff} and the turbulent mixing velocity u', the following formulation is obtained:

$$\frac{dQ_{B.Diff}}{dt} = \frac{\sqrt{c_G \cdot {c_m}^2 + c_{Kin} \cdot k}}{\sqrt[3]{\frac{V_{cyl}}{\lambda \cdot n_{nozzle}}}} \cdot m_{FuelVap} \cdot H_U \tag{16}$$

The turbulent kinetic energy k is calculated using the following equation based on a k-ε model [10]:

$$\frac{dk}{dt} = -\frac{2}{3} \cdot \frac{k}{V_{cyl}} \cdot \frac{dV_{cyl}}{dt} - \varepsilon_{Diss} \cdot \frac{k^{1,5}}{l} + \left(\varepsilon_q \cdot \frac{k_q^{1,5}}{l} \right)_{\phi > ZOT} + \varepsilon_E \cdot \frac{dk_E}{dt} + \varepsilon_D \cdot \frac{c_m^3}{l} \tag{17}$$

It is assumed that premixed and diffusion-controlled combustion start simultaneously.

In this case, a time-delay function $F_{Pre-Diff}$ is introduced to shift the diffusion combustion rate and to account for the delayed chemical reactions governing diffusion-controlled combustion immediately after the start of combustion [8]:

$$F_{Pre-Diff} = \left(\frac{m_{FuelBurn\ pre}}{m_{FuelVap\ pre}} \right)^{e} \tag{18}$$

Considering this delay function, the total heat release rate is given by:

$$\frac{dQ_{B.Diff}}{dt} = \frac{dQ_{B.Pre}}{dt} + F_{Pre-Diff} \cdot \frac{dQ_{B.Diff}}{dt} \tag{19}$$

Figure 2 illustrates the individual heat release functions as well as their superposition.

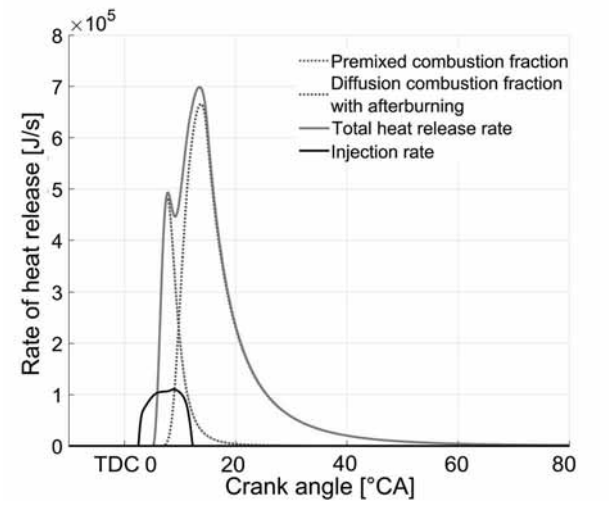

Figure 2: Modeling heat release rate.

1.2 Heat transfer model

One of the most complex submodels is the description of heat transfer between the working gas in the combustion chamber and the chamber walls.

In general, the wall heat flux in the cycle simulation is calculated using a Newtonian heat transfer approach:

$$\dot{Q}_W = \alpha \cdot A(\varphi) \cdot (T_G - T_W) \tag{20}$$

In Equation (20), A denotes the heat transfer area, which is composed of the cylinder head surface, the piston crown area, and the instantaneous lateral surface of the combustion chamber depending on the piston position.

For the calculation of the heat transfer coefficient α, a model according to Bargende is applied [11]:

$$\alpha = 253,5 \cdot V_{cyl}^{-0,073} \cdot T_m^{-0,477} \cdot p_{cyl}^{0,78} \cdot w^{0,78} \cdot \Delta \tag{21}$$

The term w represents a velocity relevant for heat transfer, while the combustion-related term Δ accounts for, among other effects, the varying temperature differences between burned and unburned gas as well as a burn-rate-dependent weighting factor X.
Both terms are calculated using Equations (22) and (23):

$$w = \frac{1}{2} \cdot \sqrt{\frac{8 \cdot k}{3} + c_K^2} \tag{22}$$

$$\Delta = \left[X \frac{T_b}{T_G} \frac{T_b - T_W}{T_G - T_W} + (1 - X) \frac{T_{ub}}{T_G} \frac{T_{ub} - T_W}{T_G - T_W} \right]^2 \tag{23}$$

In Equation (22), the specific turbulent kinetic energy k is again calculated using a k-ε model.

For the temperature calculation, a single-zone approach is applied in which no explicit separation between burned and unburned zones is performed.

According to Bargende [11], the temperature of the unburned gas T_{ub} is calculated from the start of combustion (SOC) using a polytropic relationship:

$$T_{ub} = T_{G,SOC} \cdot \left(\frac{p_{cyl}}{p_{cyl,SOC}} \right)^{\left(\frac{n-1}{n} \right)} \tag{24}$$

The temperature of the burned gas T_b is then obtained as:

$$T_b = \frac{1}{X} \cdot T_G + \frac{X - 1}{X} \cdot T_{ub} \tag{25}$$

1.3 Two-zone model

In order to predict nitrogen oxide (NO) emissions, a two-zone combustion model is introduced in addition to the single-zone approach.

In this model, the combustion chamber is divided into an unburned and a burned zone, which are separated by an infinitesimally thin flame front.

A mass exchange from the unburned to the burned zone is considered using a phenomenological approach according to Kožuch [10].

According to Kožuch, the unburned zone is described by:

$$\left(\frac{V_{ub}}{V_{cyl}}\right)^{\frac{2}{3}} \cdot \frac{dQ_w}{dt} - p\frac{dV_{ub}}{dt} + \frac{dm_{ub}}{dt} \cdot (u_{ub} + R_{ub} \cdot T_{ub}) = m_{ub} \cdot \left[\frac{\partial u_{ub}}{\partial T}\frac{dT_{ub}}{dt} + \frac{\partial u_{ub}}{\partial p}\frac{dp}{dt}\right] + u_{ub} \cdot \frac{dm_{ub}}{dt} \quad (26)$$

Analogously, the energy balance of the burned zone is given by:

$$\left(1 - \left(\frac{V_{ub}}{V_{cyl}}\right)^{\frac{2}{3}}\right) \cdot \frac{dQ_w}{dt} + \frac{dQ_B}{dt} - p\frac{dV_b}{dt} - \frac{dm_{ub}}{dt} \cdot h_{ub} = m_b \cdot \left[\frac{\partial u_b}{\partial T}\frac{dT_b}{dt} + \frac{\partial u_b}{\partial p}\frac{dp}{dt} + \frac{\partial u_b}{\partial \lambda}\frac{d\lambda_b}{dt}\right] + u_b \cdot \frac{dm_b}{dt} \quad (27)$$

Additionally, a mass transfer from the unburned zone into the burned zone is considered. This represents gas that bypasses the flame front and is directly mixed into the burned zone, allowing regulation of temperature and equivalence ratio.
The corresponding mixing function g is given by [10]:

$$g = c_g \cdot \rho_{ub} \cdot u_{Turb} \cdot V_b^{\frac{2}{3}} \cdot n_{nozzle} + c_{ga} \cdot \frac{dm_B}{dt} \quad (28)$$

Together with an additional mass flow term, the total mass transfer from the unburned to the burned zone becomes:

$$\frac{dm_{ub}}{dt} = -\left[g + (1 + x_{R,st}) \cdot \lambda_F \cdot L_{st} \cdot \frac{1}{H_U} \cdot \frac{dQ_B}{dt}\right] \quad (29)$$

Figure 3 illustrates the calculated temperature curves of the unburned and burned zones in comparison with the mass-averaged temperature obtained from the single-zone model.

Based on the calculated temperature history of the burned zone and the equilibrium composition of the species, the NO concentration is determined using chemical kinetics.

The calculation is based on the extended Zeldovich mechanism [12][13], which describes NO formation as:

$$\frac{d[NO]}{dt} = k_{1,v}[O][N_2] + k_{2,v}[N][O_2] + k_{3,v}[N][OH] - k_{1,r}[NO][N] - k_{2,r}[NO][O] - k_{3,r}[NO][H] \quad (30)$$

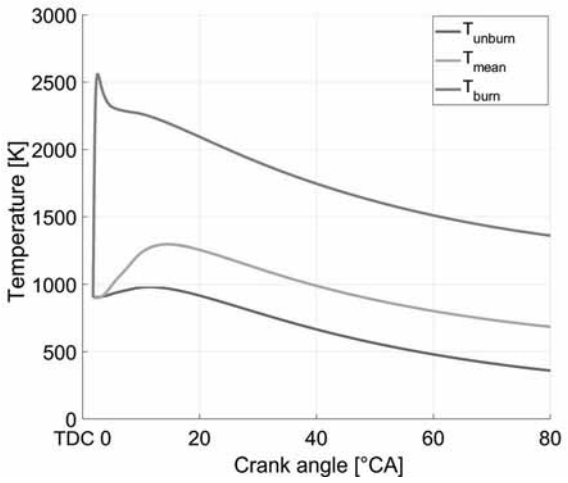

Figure 3: Temperature profiles of burned and unburned zones.

2 Turbocharger Model

In exhaust gas turbocharging, the residual exhaust gas energy available after the power stroke is utilized to increase the engine's power density. The turbine is driven by the exhaust gas enthalpy flux, which passes radially through the turbine and sets the turbine wheel and shaft into rotational motion.

This motion is transmitted to the compressor wheel, thereby supplying the internal combustion engine with an increased amount of fresh air. Considering the power balance between turbine and compressor under steady-state conditions and neglecting mechanical losses, the turbine power P_T converted from exhaust gas enthalpy equals the compressor power P_C :

$$P_T = P_C \quad (31)$$

The power of the turbine and the compressor is determined by the mass flow rate $\dot{m}_i$, the specific isentropic enthalpy difference $\Delta h_{i,is}$, and the isentropic efficiency $\eta_{i,is}$ [14]:

$$P_T = \dot{m}_T \cdot \Delta h_{T,is} \cdot \eta_{T,is} \quad (32)$$

$$P_C = \dot{m}_V \cdot \Delta h_{V,is} \cdot \frac{1}{\eta_{V,is}} \quad (33)$$

The dynamic behavior of the turbocharger is described by the power balance between turbine and compressor.

From the power difference, the rotational inertia of the rotating assembly J_{TC}, and the mechanical efficiency η_m, the change in angular velocity ω_{TC} (or rotational speed) of the turbocharger (TC) can be derived. Applying the conservation of rotational energy yields:

$$\frac{d\omega_{TC}}{dt} = \frac{P_T \cdot \eta_m - P_V}{J_{TC} \cdot \omega_{TC}} \tag{34}$$

3 Synchronous Generator

For the simulation of the generator, a per-unit (PU) based synchronous generator model from the Simscape™ library is employed [15]. The per-unit system normalizes all relevant system parameters to defined base values, resulting in dimensionless quantities. Since most generator manufacturers provide their machine parameters in per-unit notation, this approach allows for a realistic parameterization of the simulation model.

The input variable of the generator model is the rotational speed of the internal combustion engine. The output variable is the electromagnetic torque, which acts as the load torque on the combustion engine.

4 Model Validation

To evaluate the transient load behavior, the developed simulation model was validated using experimental data obtained from a test bench.

Figure 4 shows the transient response of the simulation compared to measurements for a load step from 2 kW to 13 kW. The load step is applied at a simulation time of three seconds. As a consequence of the load increase, the engine speed and thus the generator frequency decrease. The speed controller of the internal combustion engine responds by increasing the injected fuel mass, which raises the indicated torque to compensate for the increased power demand. At a simulation time of approximately seven seconds, the nominal frequency of 50 Hz is reached again and remains stable thereafter.

Overall, the simulated frequency response shows very good agreement with the experimental measurements. The gradient of the measured torque curve is slightly lower than that predicted by the simulation; however, the overall torque behavior matches the simulation results well.

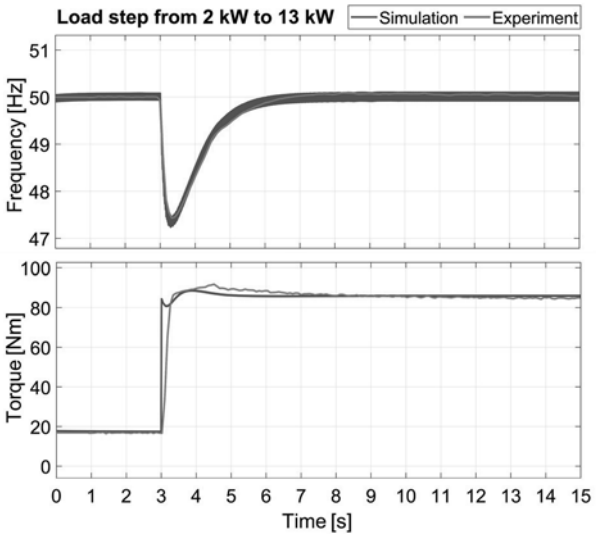

Figure 4: Simulated and measured frequency and torque response during a load step.

For further validation of the model under this load scenario, the simulation results were compared with experimental data obtained from a diesel engine test bench. Figure 5 shows a comparison of the in-cylinder pressure traces during the high-pressure phase for the load points of 2 kW and 13 kW.

In addition, the corresponding heat release rates were derived from the measured pressure traces in order to enable a direct comparison with the simulation results. The comparison of the calculated cylinder pressure and heat release curves shows very good agreement between simulation and measurement.

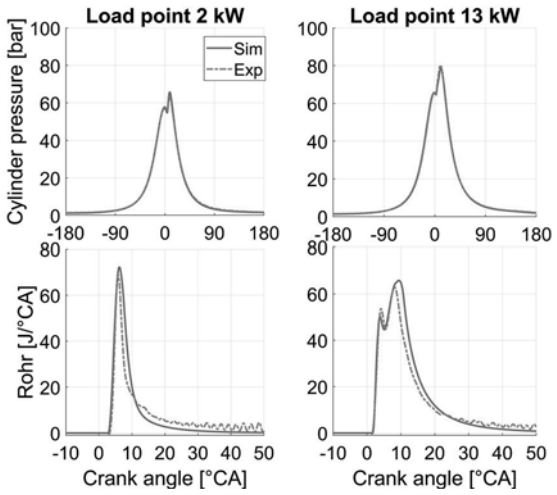

Figure 5: Comparison of in-cylinder pressure and heat release rate at 2 kW and 13 kW load points.

Figure 6 illustrates the dynamic behavior of the turbocharger during the load step using the parameters exhaust pressure, boost pressure, and turbocharger speed. The increase in injected fuel mass during the load step leads to a rise in exhaust gas enthalpy, which increases the pressure in the exhaust manifold and results in a higher turbine power output.

Consequently, the turbocharger speed increases and, due to the higher air mass flow through the compressor, the boost pressure in the intake manifold rises.

The comparison with the experimental data shows that the simulated exhaust pressure and turbocharger speed exhibit a high level of agreement with the measured curves in terms of their dynamic behavior.

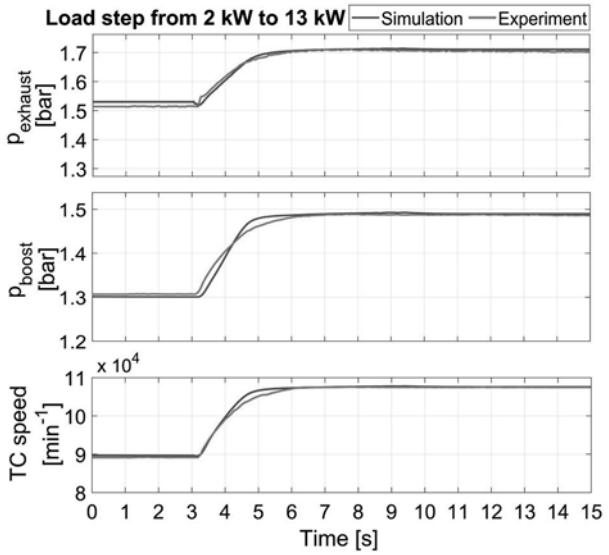

Figure 6: Exemplary transient behavior of the turbocharger (TC).

5 Summary

The modeling approach presented in this paper enables a comprehensive simulation of the operational behavior of power generation units operating in isolated grids with dynamic load conditions using a highly time-resolved process simulation.

In contrast to conventional modeling approaches, the combustion model presented here allows the simulation of multiple injection strategies due to its phenomenological formulation. In addition, the implemented two-zone model enables the prediction of nitrogen oxide emissions within the simulation framework.

The comparison of simulation results with experimental measurements from a generator test bench demonstrates very good agreement, confirming the applicability of the proposed modeling approach.

Future work will focus on investigating the influence of different fuel properties and their impact on the operational behavior of power generation units under dynamic operating conditions.

Acknowledgments

The results presented in this paper were obtained within the framework of the publicly funded project SIDYN (FKZ: 13FH043PX8) and the doctoral program of Wismar University of Applied Sciences. The authors gratefully acknowledge the financial support provided by the German Federal Ministry of Education and Research (BMBF) and Wismar University of Applied Sciences.

Publication Remark

This contribution is the revised Englisch version of the Workshop proceedings German version for **ASIM GMMS/STS 2025** - ASIM Workshop GMMS/STS 2025 - Munich/Oberpfaffenhofen 2025, published in *ASIM Workshop GMMS/STS 2025 Tagungsband* ARGESIM Report 48, e-ISBN 978-3-903347-66-3, Volume DOI 10.11128/arep.48, p 13-20.

Nomenclature

ε_{Diss}	Dissipation constant [-]
ε_D	Swirl constant [-]
ε_E	Injection constant [-]
ε_q	Squish flow constant [-]
λ	Air–fuel equivalence ratio [-]
Λ_{mc}	Air–fuel ratio mixture cloud [-]
λ_{Zn}	Local air–fuel equivalence ratio [-]
$\rho_{F,vap}$	Fuel vapor density [kg/m^3]
ρ_g	Gas density [kg/m^3]
τ_{ID}	Ignition delay [s]
$c_{0,1}$	General constant [-]
c_K	Piston speed [m/s]
c_m	Mean piston speed [m/s]
c_{pre}	Calibration parameter [m^3/(kg·s^3)]
$d_{D.eff}$	Effective nozzle diameter [mm]
e	Exponent [-]
h	Specific enthalpy [J/kg]
H_U	Lower heating value [J/kg]

k	Turbulent kinetic energy [m^2/s^2]
$k_{1,2}$	Calibration constants [-]
$k_{i,v,r}$	Reaction rate constant [$m^3/(mol \cdot s)$]
l_{Diff}	Mixing length [m]
l_l	Characteristic length [m]
L_{st}	Stoichiometric air requirement [kg/kg]
$m_{FuelVap}$	Evaporated fuel mass [kg]
m_f	Cumulative fuel mass [kg]
n	Polytropic exponent [-]
n_{Nozzle}	Number of injector holes [-]
p_0	Ambient pressure [bar]
p_{cyl}	Cylinder pressure [bar]
p_{boost}	Boost pressure [bar]
$p_{exhaust}$	Exhaust pressure [bar]
Q_B	Released heat (combustion) [J]
Q_{hyd}	Hydraulic injector flow rate [cm^3/30 s at 100 bar]
R	Specific gas constant [J/(kg·K)]
r_{mc}	Radius mixture cloud [m]
$Rohr$	Rate of heat release [J/°CA]
S_{ρ_g}	Spray penetration length at a gas density [mm]
T_{Act}	Activation temperature [K]
$T_{G,m}$	Mean in-cylinder gas temperature [K]
t_{SOC}	Start of combustion [s]
t_{SOI}	Start of injection [s]
T_W	Wall temperature [K]
u	Specific internal energy [J/kg]
u_{Drop0}	Initial droplet velocity [m/s]
u_{Turb}	Turbulent velocity [m/s]
V_{cyl}	Cylinder volume [m^3]
$x_{R,st}$	Stoichiometric residual gas fraction [-]

References

[1] Pischinger R, Klell ., Sams T. *Thermodynamik der Verbrennungskraftmaschine* 3.Auflage, Wien, SpringerWienNewYork, 2009

[2] Tschöke H, Mollenhauer K, Maier R. *Handbuch Dieselmotoren* 4.Auflage, Wiesbaden, Springer Vieweg, 2018

[3] Grill M. *Objektorientierte Prozessrechnung von Verbrennungsmotoren*, Stuttgart, University of Stuttgart, Ph.D. thesis, 2006

[4] Barba C. *Erarbeitung von Verbrennungskennwerten aus Indizierdaten zur verbesserten Prognose und rechnerischen Simulation des Verbrennungsablaufes bei Pkw-DE-Dieselmotoren mit Common-Rail Einspritzung*, Zürich, ETH Zürich, Ph.D. thesis, 2001

[5] Pirker G, Chmela F, Wimmer A. *ROHR Simulation for DI Diesel Engines Based on Sequential Combustion Mechanisms*, SAE Paper 2006-01-0654, 2006

[6] Jörss D, Ringel M, Buchholz B, Fink C. *Gekoppelte Simulation des Einspritz- und Verbrennungsvorgangs eines Industrie-Dieselmotors*, ASIM Workshop 2023 STS / GMMS / EDU, Magdeburg, 2023, DOI: 10.11128/arep21

[7] Rether D, Grill M, Schmid A, Bargende M. *Quasi-Dimensional Modeling of CI-Combustion with Multiple Pilot- and Post Injections*, SAE Paper 2010-01-0150, 2010

[8] Warth M. *Comparative investigation of mathematical methods for modeling and optimization of Common-Rail DI diesel engines*, Zürich, ETH Zürich, Ph.D. thesis, 2005

[9] Najar I, Fink C, Harndorf H, Pinker F, Buchholz B. *"Anwendungsorientierte Modelle zur Berechnung von Diesel-Sprays" in 10. Tagung Diesel- und Benzindirekteinspritzung 2016*, Wiesbaden, Springer Vieweg, 2017

[10] Kožuch, P. *Ein phänomenologisches Modell zur kombinierten Stickoxid- und Rußberechnung bei direkteinspritzenden Dieselmotoren*, Stuttgart, University of Stuttgart, Ph.D. thesis, 2004

[11] Bargende M. *Ein Gleichungsansatz zur Berechnung der instationären Wandwärmeverluste im Hochdruckteil von Ottomotoren*, Darmstadt, Technical University of Darmstadt, Ph.D. thesis, 1991

[12] Zeldovich YA. *The Oxidation of Nitrogen in Combustion and Explosions*, Acta Physicochimica, USSR, Vol.21 (577-628), 1946

[13] Lavoie GA, Heywood JB, Keck JC. *Experimental and theoretical study of nitric oxide formation in internal combustion engines*, Combustion science and technology 1970, Vol.1 (313–326)

[14] Pucher H, Zinner K. *Aufladung von Verbrennungsmotoren* 4.Auflage, Berlin Heidelberg, Springer Vieweg, 2012

[15] The MathWorks, Inc. *https://de.mathworks.com/help/sps/powersys/ref/synchronousmachinepufundamental.html*, accessed: January 14, 2025.